JACS
JOURNAL OF THE AMERICAN CHEMICAL SOCIETY

Communication

pubs.acs.org/JACS

Structural and Spectroscopic Characterization of Reaction Intermediates Involved in a Dinuclear Co–Hbpp Water Oxidation Catalyst

Carolina Gimbert-Suriñach,[†] Dooshaye Moonshiram,[‡] Laia Francàs,[†] Nora Planas,[§] Varinia Bernales,[§] Fernando Bozoglian,[†] Alexander Guda,[∥] Lorenzo Mognon,[†] Isidoro López,[†] Md Asmaul Hoque,[†] Laura Gagliardi,[§] Christopher J. Cramer,*[,§] and Antoni Llobet*[,†,⊥]

[†]Institute of Chemical Research of Catalonia (ICIQ), Barcelona Institute of Science and Technology (BIST), Av. Països Catalans 16, 43007 Tarragona, Spain

[‡]Chemical Sciences and Engineering Division, Argonne National Laboratory, 9700 South Cass Avenue, Lemont, Illinois 60439, United States

[§]Department of Chemistry, Supercomputing Institute and Chemical Theory Center, University of Minnesota, 207 Pleasant Street SE, Minneapolis, Minnesota 55455, United States

[∥]International Research Center "Smart Materials", Southern Federal University, 344090 Rostov-on-Don, Russia

[⊥]Departament de Química, Universitat Autònoma de Barcelona, 08193 Cerdanyola del Vallès, Barcelona, Spain

Supporting Information

ABSTRACT: An end-on superoxido complex with the formula $\{[Co^{III}(OH_2)(trpy)][Co^{III}(OO^{\bullet})(trpy)](\mu\text{-bpp})\}^{4+}$ ($\mathbf{3}^{4+}$) (bpp^- = bis(2-pyridyl)-3,5-pyrazolate; trpy = 2,2′;6′:2″-terpyridine) has been characterized by resonance Raman, electron paramagnetic resonance, and X-ray absorption spectroscopies. These results together with online mass spectrometry experiments using ^{17}O and ^{18}O isotopically labeled compounds prove that this compound is a key intermediate of the water oxidation reaction catalyzed by the peroxido-bridged complex $\{[Co^{III}(trpy)]_2(\mu\text{-bpp})(\mu\text{-OO})\}^{3+}$ ($\mathbf{1}^{3+}$). DFT calculations agree with and complement the experimental data, offering a complete description of the transition states and intermediates involved in the catalytic cycle.

Oxygen activation by first-row transition metal complexes in low oxidation states has been a very active field of research for the last two decades.[1] A plethora of transition metal peroxido and superoxido complexes in different coordination modes have been prepared and characterized with spectroscopic techniques and even via single-crystal X-ray diffraction in selected instances.[2] The reverse reaction, the oxidation of water to molecular oxygen assisted by first-row transition metal complexes, is a field that has emerged recently, and proper characterization of the potential peroxido and/or superoxido reaction intermediates is practically nonexistent.[3] The characterization of such intermediates is hampered by the lability of the metal–ligand bonds, which can undergo substitution by water solvent molecules, and by the relatively low temperature range at which the reaction can be operated. In sharp contrast, the inverse reaction, i.e., oxygen activation, can be carried out in organic solvents and at very low temperatures. Additionally, for the water oxidation reaction, in a number of cases a competing and/or preferential ligand oxidation occurs,[4] which prevents extraction of reliable and meaningful information. In previous work, we reported the synthesis and X-ray structure of the dinuclear μ-peroxido complex $\{[Co^{III}(trpy)]_2(\mu\text{-bpp})(\mu\text{-OO})\}^{3+}$, hereafter denoted as $\mathbf{1}^{3+}$ or $[Co^{III}\text{–}OO\text{–}Co^{III}]^{3+}$ (trpy = 2,2′;6′:2″-terpyridine; bpp^- = bis(2-pyridyl)-3,5-pyrazolate), that behaves as a powerful catalyst for the four-electron ($4e^-$) reduction of O_2 to water.[5] The key structures are depicted in Scheme 1. Further, we electrochemically characterized the properties of $\mathbf{1}^{3+}$ and showed by voltammetric and potentiometric techniques its capacity to act as a catalyst for the $4e^-$ oxidation of water to O_2.[6]

Scheme 1. Simplified (left) Oxygen Reduction and (right) Water Oxidation Catalytic Cycles Based on the Co–Hbpp Complex and (center, red-shaded) the Intermediates Shared by the Two Catalytic Cycles ($\mathbf{1}^{3+}$ and $\mathbf{5}^{4+}$)

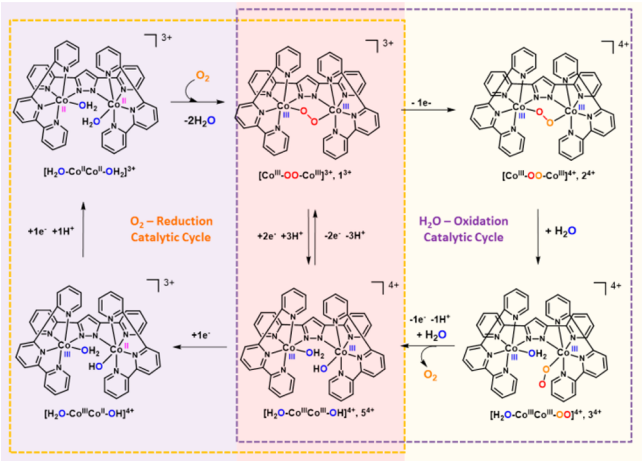

Received: August 15, 2016
Published: November 8, 2016

DOI: 10.1021/jacs.6b08532
J. Am. Chem. Soc. 2016, 138, 15291–15294

Here we present the preparation of a dinuclear Co superoxido end-on complex, denoted as $\mathbf{3}^{4+}$ or $[H_2O{-}Co^{III}Co^{III}{-}OO^{\bullet}]^{4+}$, and its thorough characterization by vibrational, X-ray absorption near edge structure (XANES), extended X-ray absorption fine structure (EXAFS), and electron paramagnetic resonance (EPR) spectroscopies together with density functional theory (DFT) calculations. We show for the first time that sequential oxidation of the peroxido derivative $\mathbf{1}^{3+}$ leads to the just-mentioned superoxido $\mathbf{3}^{4+}$ and that further oxidation of the latter generates O_2. These two reactions have been carried out using ^{16}O-, ^{17}O-, and ^{18}O-labeled complexes to properly characterize potential intermediates. We also present a coherent mechanistic description of the catalytic cycle based on DFT calculations that agree with the available experimental data.

The dinuclear Co μ-peroxido complex $\mathbf{1}^{3+}$ was prepared in good yields following literature procedures by reacting $\{[Co^{II}(OH_2)(trpy)]_2(\mu\text{-bpp})\}^{3+}$ or its chlorido-bridged derivative with molecular O_2 (Scheme 1).[5] Using O_2 labeled with different isotopes (^{16}O, ^{17}O, or ^{18}O), we prepared the peroxido complexes $\mathbf{1(32)}^{3+}$ $[Co^{III}{-}^{16}O^{16}O{-}Co^{III}]^{3+}$, $\mathbf{1(34)}^{3+}$ $[Co^{III}{-}^{17}O^{17}O{-}Co^{III}]^{3+}$, and $\mathbf{1(36)}^{3+}$ $[Co^{III}{-}^{18}O^{18}O{-}Co^{III}]^{3+}$, respectively. Figure 1 (left) shows the resonance Raman (rR)

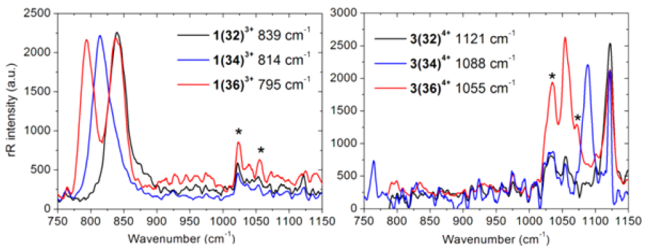

Figure 1. Normalized rR spectra of (left) the peroxido complexes $\mathbf{1(32)}^{3+}$ (black), $\mathbf{1(34)}^{3+}$ (blue), and $\mathbf{1(36)}^{3+}$ (red) and (right) the superoxido complexes $\mathbf{3(32)}^{4+}$ (black), $\mathbf{3(34)}^{4+}$ (blue), and $\mathbf{3(36)}^{4+}$ (red). λ_{exc} = 514 nm. Asterisks indicate solvent resonances.

spectra obtained for the $\mathbf{1}^{3+}$ set of complexes with the different labeling. A prominent peak appears at 839 cm^{-1} for $\mathbf{1(32)}^{3+}$ associated with the O−O bond stretching mode. This peak shifts to 814 cm^{-1} for $\mathbf{1(34)}^{3+}$ and to 795 cm^{-1} for $\mathbf{1(36)}^{3+}$, as expected for a quantum-mechanical harmonic oscillator having such changes in reduced mass. The rR spectrum of $\mathbf{1(36)}^{3+}$ shows the presence of two bands at 839 and 795 cm^{-1} with similar intensities that are due to a 1:1 ratio of $\mathbf{1(32)}^{3+}$ and $\mathbf{1(36)}^{3+}$ since the O_2 used in the synthesis was a 1:1 $^{36}O_2/^{32}O_2$ mixture (see the Supporting Information (SI)). Similarly, the ^{17}O labeling experiment, which used a 9:1 $^{34}O_2/^{32}O_2$ mixture, shows a small shoulder at 839 cm^{-1} in the corresponding rR spectrum.

Chemically, the addition of 1 equiv of Ce^{IV} to the peroxido complexes $\mathbf{1}^{3+}$ at pH 1.0 generates the corresponding superoxido complexes $\mathbf{2}^{4+}$ or $[Co^{III}{-}O^{\bullet}O{-}Co^{III}]^{4+}$, which undergo hydrolysis to yield end-on superoxido complexes $\mathbf{3}^{4+}$ or $[H_2O{-}Co^{III}Co^{III}{-}OO^{\bullet}]^{4+}$, as suggested by DFT calculations and in agreement with XAS spectroscopy. DFT calculations at the SMD(water)/M11-L/6-311G(2f,d) level predict that the end-on form $\mathbf{3}^{4+}$ is 19.8 kcal/mol more stable than the bridging form $\mathbf{2}^{4+}$ (Scheme 2). Figure 2 (right) shows the optimized DFT structure for the end-on superoxido complex together with the singly occupied molecular orbital (SOMO). The spin density in this orbital is mainly localized on the superoxido group, which forms a hydrogen bond with the neighboring Co−OH_2 group supporting the peroxido bridge as the main oxidation site. Previous

Scheme 2. Calculated Water Oxidation Catalytic Cycle Associated with the Co−Hbpp Complex[a]

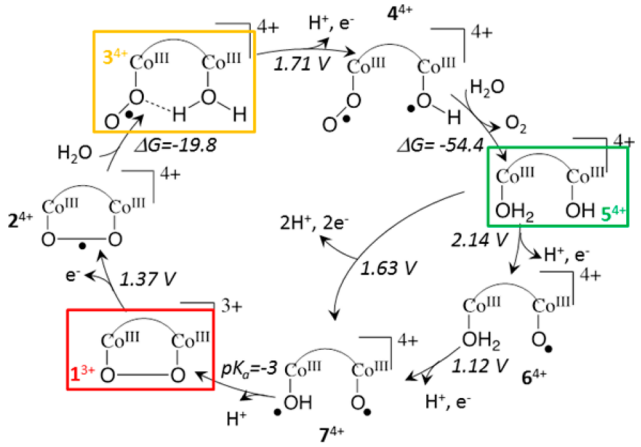

[a]The arc connecting the two Co centers represents the bpp$^-$ bridging ligand. For clarity, the trpy ligands are not shown. Red box: starting material $[Co^{III}{-}OO{-}Co^{III}]^{3+}$, $\mathbf{1}^{3+}$. Yellow box: hydrated one-electron oxidation product $[H_2O{-}Co^{III}Co^{III}{-}OO^{\bullet}]^{4+}$, $\mathbf{3}^{4+}$. Green box: $[H_2O{-}Co^{III}Co^{III}{-}OH]^{4+}$, $\mathbf{5}^{4+}$, the species formed after oxygen ejection. Potentials are in V vs NHE at pH 2.0, and ΔG values are in kcal/mol.

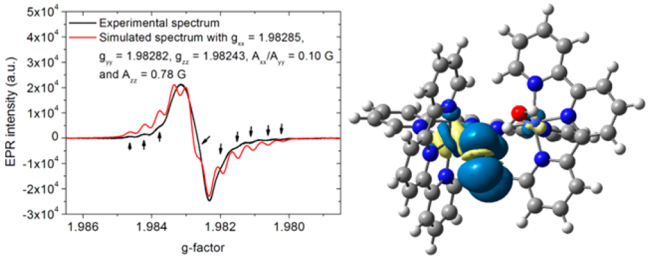

Figure 2. (left) Experimental (black) and simulated (red) EPR spectra of $\mathbf{3(34)}^{4+}$. (right) SOMO of end-on superoxido complex $\mathbf{3(32)}^{4+}$.

electrochemical experiments showed that the oxidation of the peroxido complex $\mathbf{1}^{3+}$ to the superoxido $\mathbf{3}^{4+}$ is chemically and electrochemically reversible and occurs at $E^{\circ\prime}$ = 1.49 V vs NHE.[6] DFT calculations using again SMD(water)/M11-L/6-311G-(2f,d) predict a value of 1.37 V vs NHE for this oxidation in good agreement with the experimental value and thus suggests that this level of theory will be useful and sufficiently accurate for modeling other properties of the system.

Vibrational rR spectroscopy was also carried out for the superoxido complexes with the different O_2 isotopologues, and the results are shown in Figure 1 (right). The O−O bond vibration for the $\mathbf{3(32)}^{4+}$ oxidized complex appears at 1121 cm^{-1}, which is consistent with a superoxido group,[7] although experimentally the end-on and side-on isomers are virtually indistinguishable.[7d,8] This peak shifts to 1088 and 1055 cm^{-1} for $\mathbf{3(34)}^{4+}$ and $\mathbf{3(36)}^{4+}$, respectively, as expected. Here again, the mixture of isomers is clearly observed in the spectra, since we used the peroxido complexes mentioned earlier as starting materials. It is worth noting here that the potential use of mixed labeled O atoms would generate one band for the symmetric side-on complex (Co−$O^{16}O^{18}$−Co) and two for the end-on complex (CoCo−$O^{16}O^{18}$ and CoCo−$O^{18}O^{16}$). However, the energy difference for the two bands in the latter case would be too small to be clearly differentiated in the spectrum (theory predicts a shift of 1−3 cm^{-1} for related complexes).[8]

DOI: 10.1021/jacs.6b08532
J. Am. Chem. Soc. 2016, 138, 15291−15294

The superoxido complexes were also characterized by EPR spectroscopy. For complexes $\mathbf{3(32)}^{4+}$ and $\mathbf{3(36)}^{4+}$ a broad band centered at $g = 1.98$ is observed in the EPR spectrum, which is due to the unpaired electron of the superoxido group. The broadness of the peaks is a consequence of the coupling of the superoxido unpaired electron with the nuclear spin of ^{59}Co ($I = {}^{7}/_{2}$), which is not well resolved (see Figure S1). In sharp contrast, $\mathbf{3(34)}^{4+}$ shows an EPR spectrum similar to that of $\mathbf{3(32)}^{4+}$ but with fine structure due to the coupling to the nuclear spin of ^{17}O ($I = {}^{5}/_{2}$) (Figure 2, left).

XANES analysis of the superoxido complex $\mathbf{3}^{4+}$ reveals a small positive shift of the rising edge (0.4 eV) compared with peroxido $\mathbf{1}^{3+}$ (Figure 3, top left). The shift in energy indicates a change in the electron density and local geometry around the Co metal center and is well-reproduced by theoretical XANES simulations, as shown in Figure 3 (right), thus supporting a peroxido-centered oxidation in agreement with the rR and EPR results. More interestingly, a predominant characteristic multiplet feature is observed in the pre-edge region that distinguishes the superoxido compound from its parent peroxido derivative (Figure 3, bottom). The presence of pre-edge features corresponds to the 1s-to-3d quadrupole transitions and dipole excitations of the core electrons into the valence 3d levels hybridized with p orbitals.[9] Upon oxidation with 1 equiv of Ce^{IV}, local distortions around the Co center and increased hybridization of the valence 3d states with ligand N/O p orbitals result in the clear formation of a second pronounced pre-edge feature. As shown by the Gaussian fits in Figure 3 (bottom), the pre-edge region has contributions from two main absorptions centered at ca. 7709.9 and 7712.2 eV for the peroxido derivative. Upon oxidation, the peak at 7712.2 eV slightly shifts to higher energy (7712.7 eV) and becomes more pronounced, giving rise to an apparent doublet feature that is not as obvious for the starting peroxido compound (compare the black and red traces). Theoretical DFT-MO XANES calculations of the superoxido derivatives $\mathbf{2}^{4+}$ and $\mathbf{3}^{4+}$ in Scheme 2 reproduce this shift well, especially for the nonsymmetric end-on compound $\mathbf{3}^{4+}$, where the doublet feature is more noticeable (Figures 3 and S3). In addition, EXAFS analysis shows a slightly better fit for $\mathbf{3}^{4+}$ (see the SI). Previous electrochemical experiments revealed that the superoxido complex $\mathbf{3}^{4+}$ can be further oxidized by one electron at 1.80 V vs NHE.[6] M11-L DFT calculations suggest the formation of a diradical hydroxyl–superoxido species $[HO^{\bullet}-Co^{III}Co^{III}-OO^{\bullet}]^{4+}$ ($\mathbf{4}^{4+}$) obtained from a proton-coupled electron transfer (PCET) process occurring at a potential of 1.71 V vs NHE (Scheme 2). This new redox couple ($\mathbf{3}^{4+}/\mathbf{4}^{4+}$) is responsible for a large electrocatalytic wave in the 1.8–2.0 V vs NHE potential range associated with catalytic oxidation of water to O_2.[6] In agreement with these electrochemical results, further addition of Ce^{IV} to the superoxido complexes $\mathbf{3}^{4+}$ should generate O_2. Indeed, Figure 4 shows the online mass spectrometry (MS) results of adding 4 equiv of Ce^{IV} to a solution of $\mathbf{1(34)}^{3+}$, which generates a ca. 10:1 $^{34}O_2$:$^{32}O_2$ mixture, in very good agreement with the expected 9:1 ratio of the starting materials. $\mathbf{3(32)}^{4+}$ and $\mathbf{3(36)}^{4+}$ also give the expected ratios of labeled O_2 (Figure S8).

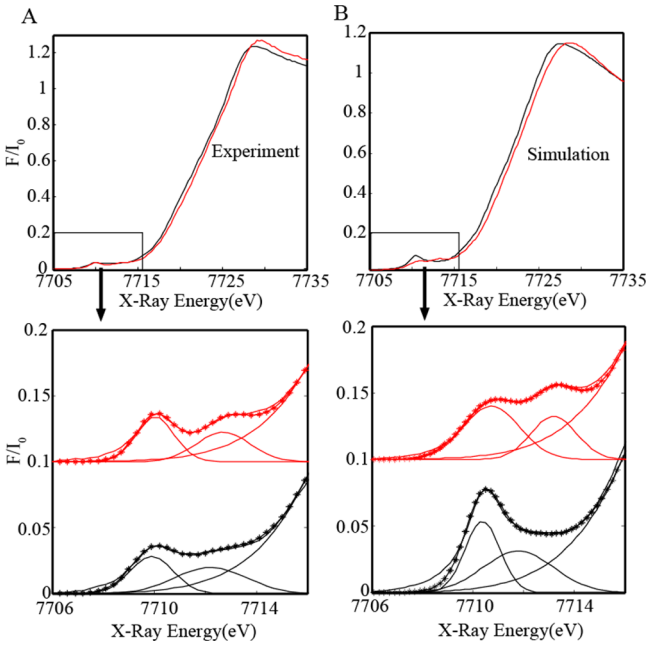

Figure 3. XANES spectra of $\mathbf{1(32)}^{3+}$ (black) and $\mathbf{3(32)}^{4+}$ (red). (A) (top) Experimental results and (bottom) zoomed view of the pre-edge regions and Gaussian fits of the two pre-edge peaks. (B) (top) DFT-MO simulated data and (bottom) zoomed view of the pre-edge region and Gaussian fits of the two pre-edge peaks. Also see Figure S3.

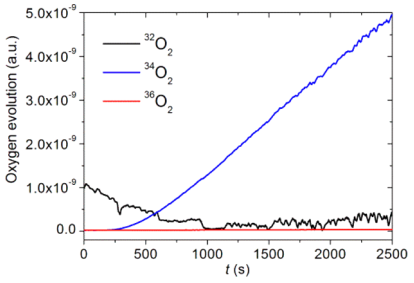

Figure 4. O_2 evolution profile for a mixture containing $\mathbf{1(34)}^{3+}$ and 4 equiv of $(NH_4)_2Ce(NO_3)_6$ in 0.1 M triflic acid (pH 1.0).

Further DFT calculations were undertaken to complete the catalytic cycle (Scheme 2). Oxygen ejection from $\mathbf{4}^{4+}$ concomitant with solvent coordination generates a dicobalt(III) aqua–hydroxo complex, $[HO-Co^{III}Co^{III}-OH_2]^{4+}$ ($\mathbf{5}^{4+}$). Species $\mathbf{5}^{4+}$ is predicted to be further oxidized by a two-electron/two-proton single step at a potential of 1.63 V vs NHE (which is slightly lower than that required for the oxidation of $\mathbf{3}^{4+}$ to $\mathbf{4}^{4+}$) to generate the highly reactive oxyl–hydroxyl species $[HO^{\bullet}-Co^{III}Co^{III}-O^{\bullet}]$ ($\mathbf{7}^{4+}$). The aqueous pK_a of $\mathbf{7}^{4+}$ is predicted to be −3, so proton loss to generate the initial peroxido species $\mathbf{1}^{3+}$ is expected to be spontaneous. Indeed, it cannot be ruled out that the oxidation of $\mathbf{5}^{4+}$ may occur as an overall two-electron/three-proton step, as we have not attempted to model the specific kinetics of these PCET transformations. The resulting bis[cobalt(III)–oxyl] compound, $\mathbf{7}^{4+}$, is predicted not to be stationary at the M11/L level but to spontaneously form an O–O bond leading to the bridged peroxido complex $\mathbf{1}^{3+}$, closing the catalytic cycle. Theory indicates that $\mathbf{7}^{4+}$ should have an extremely short lifetime, thereby disfavoring O–O bond formation through nucleophilic attack of water on the oxyl fragment. It is interesting to note here the fundamental role played by the bpp^{-} ligand in maintaining the two metal centers in close proximity. In the O–O bond formation step, the ligand preorganizes the two Co–O moieties in $\mathbf{7}^{4+}$ so that the O–O bond formation is entropically favored. Further, the last step before oxygen ejection involves the formation of a diradical hydroxyl–superoxido species $\mathbf{4}^{4+}$, where the Co–O$^{\bullet}$H and the Co–OO$^{\bullet}$ moieties are situated in close proximity. Electron transfer to the cobalt hydroxyl moiety from the superoxido ligand is then ultimately responsible for the oxygen ejection. The needed

DOI: 10.1021/jacs.6b08532
J. Am. Chem. Soc. 2016, 138, 15291–15294

generation of a Co−hydroxyl simultaneously with a Co−superoxido cannot occur at a single site, as would be required in a mononuclear complex. It should also be noticed that the water oxidation reaction cycle involves oxygen-only (not metal-centered) redox processes involving the superoxido and aqua ligands in different protonation states (i.e., oxyl or hydroxyl radicals). The Co^{III} centers act as scaffolds that strategically support the reactive oxygen radical species but do not undergo metal-centered redox processes.

Scheme 1 shows the interplay between the oxygen reduction and water oxidation catalytic cycles for the Co−Hbpp complex. The two catalytic cycles share two common reactive intermediates, $[Co^{III}-OO-Co^{III}]^{3+}$ $\mathbf{1}^{3+}$ and $[H_2O-Co^{III}Co^{III}-OH]^{4+}$ $\mathbf{5}^{4+}$ (shown at the center of Scheme 1 and whose X-ray structures have been described previously).[5,6] Oxidation of $[Co^{III}-OO-Co^{III}]^{3+}$ leads to the water oxidation cycle (yellow box in Scheme 1), whereas reduction of $[H_2O-Co^{III}Co^{III}-OH]^{4+}$ leads to the oxygen reduction cycle (purple box in Scheme 1). The use of similar types of species for O−O bond formation and O−O bond cleavage but at different oxidation states parallels the chemistry that occurs at chloride dismutase (Chl-D)[10] and Cyt-P450,[11] respectively, in nature. In the Cyt-P450 cycle, the Fe(II) porphyrin active center reacts with oxygen to generate an Fe(III)−superoxido species that eventually leads to O−O bond scission, forming a high-oxidation-state Fe^{IV}═O species responsible for organic substrate oxidations. On the other hand, in the catalytic cycle proposed for Chl-D, the lowest oxidation state proposed for the Fe porphyrin is III, at which point molecular oxygen is released.

In conclusion, we have reported the detailed characterization of reaction intermediates involved in the catalytic cycle of a first-row transition-metal-based water oxidation catalyst. This work is also important because it can be taken as a low-molecular-weight model of cobalt oxides,[12,3b] although it is worth noting that the electronic coupling through the bpp^- ligand can be significantly different from that of oxo-bridged cobalt oxides. The latter together with nickel oxides are among the most active earth-abundant water oxidation heterogeneous catalysts.[12a,13] For those oxides, thorough structural characterizations and mechanistic studies of active species are inherently difficult given their heterogeneous nature. In addition, we have also shown that the same transition metal complex can be used for both the water oxidation and oxygen reduction catalytic reactions.

■ ASSOCIATED CONTENT

Supporting Information

The Supporting Information is available free of charge on the ACS Publications website at DOI: 10.1021/jacs.6b08532.

Spectroscopic and computational details (PDF)

■ AUTHOR INFORMATION

Corresponding Authors

*cramer@umn.edu; Twitter: @ChemProfCramer

*allobet@iciq.cat

Notes

The authors declare no competing financial interest.

■ ACKNOWLEDGMENTS

Financial support from MINECO and FEDER (CTQ-2016-80058-R, SEV-2013-0319, and CTQ-2014-52974-REDC) and EU COST Actions CM1202 and CM1205 is acknowledged. D.M. thanks the U.S. Department of Energy (DOE), Office of Science, Office of Basic Energy Sciences (BES), CSGB Division (Contract DE-AC02-06CH11357) and resources of the Advanced Photon Source (APS) and Center of Nanoscale Materials both at Argonne National Laboratory (ANL). Dr. Sun from Sector 20 (APS), supported by U.S. DOE and the Canadian Light Source, is also acknowledged. C.J.C. thanks the U.S. NSF for support (CHE-1361595). L.G. was partially supported by the U.S. DOE, Basic Energy Sciences, under SciDAC (Grant No. DE-SC0008666). A.G. thanks the Russian Ministry of Education and Science for the financial support (Agreement No. 14.587.21.0002, unique identifier RFMEFI58714X0002).

■ REFERENCES

(1) (a) Hematian, S.; Garcia-Bosch, I.; Karlin, K. D. *Acc. Chem. Res.* **2015**, *48*, 2462. (b) Nam, W. *Acc. Chem. Res.* **2015**, *48*, 2415. (c) Cramer, C. J.; Tolman, W. B. *Acc. Chem. Res.* **2007**, *40*, 601. (d) Citek, C.; Herres-Pawlis, S.; Stack, T. D. P. *Acc. Chem. Res.* **2015**, *48*, 2424.

(2) (a) Cho, J.; Jeon, S.; Wilson, S. A.; Liu, L. V.; Kang, E. A.; Braymer, J. J.; Lim, M. H.; Hedman, B.; Hodgson, K. O.; Valentine, J. S.; Solomon, E. I.; Nam, W. *Nature* **2011**, *478*, 502. (b) Bukowski, M. R.; Koehntop, K. D.; Stubna, A.; Bominaar, E. L.; Halfen, J. A.; Münck, E.; Nam, W.; Que, L., Jr. *Science* **2005**, *310*, 1000.

(3) (a) Concepcion, J. J.; Tsai, M.-K.; Muckerman, J. T.; Meyer, T. J. *J. Am. Chem. Soc.* **2010**, *132*, 1545. (b) Zhang, M.; de Respinis, M.; Frei, H. *Nat. Chem.* **2014**, *6*, 362.

(4) (a) Wang, J.-W.; Sahoo, P.; Lu, T.-B. *ACS Catal.* **2016**, *6*, 5062. (b) Hoffert, W. A.; Mock, M. T.; Appel, A. M.; Yang, J. Y. *Eur. J. Inorg. Chem.* **2013**, *2013*, 3846. (c) Radaram, B.; Ivie, J. A.; Singh, W. M.; Grudzien, R. M.; Reibenspies, J. H.; Webster, C. E.; Zhao, X. *Inorg. Chem.* **2011**, *50*, 10564.

(5) Fukuzumi, S.; Mandal, S.; Mase, K.; Ohkubo, K.; Park, H.; Benet-Buchholz, J.; Nam, W.; Llobet, A. *J. Am. Chem. Soc.* **2012**, *134*, 9906.

(6) Rigsby, M. L.; Mandal, S.; Nam, W.; Spencer, L. C.; Llobet, A.; Stahl, S. S. *Chem. Sci.* **2012**, *3*, 3058.

(7) (a) Barraclough, C. G.; Lawrance, G. A.; Lay, P. A. *Inorg. Chem.* **1978**, *17*, 3317. (b) Schmidt, S.; Heinemann, F. W.; Grohmann, A. *Eur. J. Inorg. Chem.* **2000**, *2000*, 1657. (c) Rajani, C.; Kincaid, J. R.; Petering, D. H. *J. Am. Chem. Soc.* **2004**, *126*, 3829. (d) Nakamoto, K. *Infrared and Raman Spectra of Inorganic and Coordination Compounds*, 6th ed.; John Wiley & Sons: Hoboken, NJ, 2009.

(8) (a) Kinsinger, C. R.; Gherman, B. F.; Gagliardi, L.; Cramer, C. J. *JBIC, J. Biol. Inorg. Chem.* **2005**, *10*, 778. (b) Shan, X.; Que, L., Jr. *Proc. Natl. Acad. Sci. U. S. A.* **2005**, *102*, 5340.

(9) (a) Loeb, K. E.; Westre, T. E.; Kappock, T. J.; Mitic, N.; Glasfeld, E.; Caradonna, J. P.; Hedman, B.; Hodgson, K. O.; Solomon, E. I. *J. Am. Chem. Soc.* **1997**, *119*, 1901. (b) Westre, T. E.; Kennepohl, P.; DeWitt, J. G.; Hedman, B.; Hodgson, K. O.; Solomon, E. I. *J. Am. Chem. Soc.* **1997**, *119*, 6297. (c) de Groot, F. *Chem. Rev.* **2001**, *101*, 1779. (d) Chandrasekaran, P.; Stieber, S. C. E.; Collins, T. J.; Que, L., Jr.; Neese, F.; DeBeer, S. *Dalton Trans.* **2011**, *40*, 11070.

(10) (a) Mlynek, G.; Sjöblom, B.; Kostan, J.; Füreder, S.; Maixner, F.; Gysel, K.; Furtmüller, P. G.; Obinger, C.; Wagner, M.; Daims, H.; Djinović-Carugo, K. *J. Bacteriol.* **2011**, *193*, 2408. (b) Sun, S.; Li, Z.-S.; Chen, S.-L. *Dalton Trans.* **2014**, *43*, 973.

(11) (a) Ener, M. E.; Lee, Y.-T.; Winkler, J. R.; Gray, H. B.; Cheruzel, L. *Proc. Natl. Acad. Sci. U. S. A.* **2010**, *107*, 18783. (b) Guengerich, F. P. *J. Biochem. Mol. Toxicol.* **2007**, *21*, 163.

(12) (a) McCrory, C. C. L.; Jung, S.; Ferrer, I. M.; Chatman, S. M.; Peters, J. C.; Jaramillo, T. F. *J. Am. Chem. Soc.* **2015**, *137*, 4347. (b) Nguyen, A. I.; Ziegler, M. S.; Oña-Burgos, P.; Sturzbecher-Hohne, M.; Kim, W.; Bellone, D. E.; Tilley, T. D. *J. Am. Chem. Soc.* **2015**, *137*, 12865. (c) Coehn, A.; Gläser, M. *Zeit. Anorg. Chem.* **1902**, *33*, 9.

(13) (a) Hu, S.; Shaner, M. R.; Beardslee, J. A.; Lichterman, M.; Brunschwig, B. S.; Lewis, N. S. *Science* **2014**, *344*, 1005. (b) Kenney, M. J.; Gong, M.; Li, Y.; Wu, J. Z.; Feng, J.; Lanza, M.; Dai, H. *Science* **2013**, *342*, 836.

DOI: 10.1021/jacs.6b08532
J. Am. Chem. Soc. 2016, 138, 15291−15294